Water Resources Research

RESEARCH ARTICLE
10.1029/2022WR033114

Experimental Observations of Bedload Tracer Movement: Effects of Mixed Particle Sizes and Bedforms

Arvind Singh[1], Zi Wu[1,2], Peter Wilcock[3], and Efi Foufoula-Georgiou[4,5]

[1]Department of Civil, Environmental and Construction Engineering, University of Central Florida, Orlando, FL, USA, [2]State Key Laboratory of Hydro science and Engineering, Department of Hydraulic Engineering, Tsinghua University, Beijing, China, [3]Department of Watershed Sciences, Utah State University, Logan, UT, USA, [4]Department of Civil and Environmental Engineering, University of California Irvine, Irvine, CA, USA, [5]Department of Earth System Science, University of California Irvine, Irvine, CA, USA

Key Points:

- Bedforms serve as a primary control on tracer travel distances
- Bedform trap efficiency depends linearly on the relative bedform height
- Travel distances of a mixture of particles and under variable discharge exhibit a heavy-tailed distribution

Correspondence to:

A. Singh and Z. Wu,
Arvind.Singh@ucf.edu;
wuzi@tsinghua.edu.cn

Citation:

Singh, A., Wu, Z., Wilcock, P., & Foufoula-Georgiou, E. (2023). Experimental observations of bedload tracer movement: Effects of mixed particle sizes and bedforms. *Water Resources Research*, *59*, e2022WR033114. https://doi.org/10.1029/2022WR033114

Received 27 JUN 2022
Accepted 24 APR 2023

Abstract Predicting the transport of bedload tracer particles is a problem of significant theoretical and practical interest. Yet, little understanding exists for transport in rivers in the presence of bedforms, which may trap grains and thereby influence travel distance. In a series of flume experiments with a sandy gravel bed in a large experimental flume, bed elevation and tracer travel distances were measured at high resolution for a range of discharges. As discharge increased, bedform height increased and bedform length decreased, increasing bedform steepness. For all tracer sizes and flow conditions, bedforms act as primary controls on the tracer travel distances. Bedform trapping increases linearly with the ratio of bedform height to tracer grain size, with 50% trapping efficiency for a ratio of two and 90% trapping efficiency for a ratio of four. A theoretical model based on the extended active layer formulation for sediment transport is able to capture much of the distribution of measured travel distances for all tracer sizes and discharges, providing a first connection between tracer transport theory and bedform trapping and indicating normal diffusion of tracers at relatively small timescales. Variable bedform geometry can influence trap efficiency for individual bedforms and the theoretical model can help identify "preferential trapping" conditions. The distribution of tracer travel distances for a mixture of grain sizes and variable discharge, as expected in natural rivers, displays heavy tail characteristics.

1. Introduction

Heterogeneities due to particle-scale dynamics of bedload transport significantly affect the geomorphology, hydrology, hydraulics and ecology of gravel-bed streams and consequently alter the nutrient, pollutant, and microorganism transport (Li et al., 2023; Mao et al., 2011; Nelson et al., 2009; Orr et al., 2009; Wu et al., 2023; Yarnell et al., 2006). Therefore, knowledge of particle-scale dynamics of bedload transport and its relationship to macroscale bed topography is vital for accurately predicting sediment transport in gravel-bed rivers.

Previous work has shown that bedload transport depends on flow strength and is highly stochastic (Ancey, 2010; Ancey et al., 2008; Einstein, 1937, 1950; Gomez et al., 1989; Hassan et al., 1991; Paintal, 1971; Pierce & Hassan, 2020b; Singh, Fienberg, et al., 2009; Singh, Lanzoni, & Foufoula-Georgiou, 2009; Singh et al., 2010). Although several proposed theories of stochastic sediment transport have reproduced a number of statistical properties of bedload transport and particle movement (Ancey, 2010; Ancey et al., 2008; Church & Hassan, 1992; Einstein, 1937, 1950; Furbish et al., 2012; Ganti et al., 2009, 2010; Hassan et al., 1991; Paintal, 1971; Pierce & Hassan, 2020a; Pretzlav et al., 2021; Roseberry et al., 2012; Wong et al., 2007), a more rigorous validation of these models is still lacking for the range of transport conditions observed in nature, including a varying hydrograph and evolving bed topography.

For natural rivers, the motion of individual particles is difficult to measure with direct bedload sampling, an issue that has inspired an interest in field gravel tracer studies in the last two decades (Church & Hassan, 1992; Ergenzinger et al., 1989; Habersack, 2001; Hassan, 1990; Hassan et al., 1991; Wilcock, 1997). Technological advances in high frequency radio tracking and magnetic tracers have enabled the direct measurement of particle displacements (or travel distances) and rest periods (or waiting times) in natural sedimentary systems (Bradley, 2017; Chacho et al., 1989; Church & Hassan, 1992; Ergenzinger et al., 1989; Habersack, 2001; Hassan et al., 1991; Phillips et al., 2013). Furthermore, for logistics and safety considerations in the field, tracer particles can be deployed during low-flow conditions to avoid direct sampling of bedload transport rates during high flows and floods (Wilcock, 1997).

Discriminating among statistical (i.e., exponential, Gamma, lognormal) distributions of waiting times and step lengths for individual particles is important in the formulation of stochastic models of bedload transport (Einstein, 1937, 1950; Ganti et al., 2010; Hill et al., 2010; Kleinhans & Rijn, 2002; McEwan et al., 2004; Wong et al., 2007; Wu, Singh, et al., 2019). Ideally, the stochastic motion of a single bedload grain, driven by particle-particle and/or fluid-particle interactions and consisting of a series of stops and starts, can be well-documented with tracer particles. However, instead of identifying every pair of starting and ending positions for the tracer particle during transport so as to document step lengths (and associated waiting times), current techniques applied to field experiments only allow measurements of the total distance traveled during a given time period, leading to acquisition of coarser information of travel distances (Bradley, 2017; Phillips et al., 2013). The resulting distributions of travel distances are typically strongly skewed with peaks (modes) close to the point of tracer release, which is due to either no tracer movement or small movement in the downstream direction.

Regarding laboratory experiments, there have been studies focusing on processes at the flume scale to link tracer displacement to macroscopic bulk bedload transport (Wilcock, 1997; Wong et al., 2007). High precision tracer tracking experiments have also been developed tracking moving particles with high-speed imagery techniques, with frequencies as high as hundreds of frames per second, allowing recording and extracting complete tracer trajectories (Ancey & Heyman, 2014; Martin et al., 2012; Roseberry et al., 2012; Wu et al., 2020). Such experiments focusing on particle scale processes not only enable direct measurements of step lengths, but also provide much more detailed information for the kinematics of particles, leading to new formulations for particle motions (Ancey & Heyman, 2014; Wu et al., 2020, 2021) and evidence of thin-tailed step length distributions (Wu et al., 2020).

Flume tracer studies to date have been mainly conducted under plane-bed conditions. Bed forms are likely to play an important role in controlling particle displacement in both sand-bed and gravel-bed systems. To the best of our knowledge, only a couple of studies have focused on quantifying the effect of bedforms on tracer movement in gravel bed environments (Hassan, 1990; Pyrce & Ashmore, 2003). Using magnetically tagged tracer particles in two natural streams, Hassan (1990) showed that the distribution of buried tagged particles varied spatially both within a bedform and from one bedform to another (see also Hassan et al. (1991)). Others have demonstrated that larger scale features such as alternate bars and point bars can determine tracer travel distance. For example, Pyrce and Ashmore (2003) showed that more than 50% of the bedload tracer particles were deposited on the first point bar encountered in a laboratory flume (see also Hassan and Bradley (2017)). In sand bed rivers, some studies have explored the effect of bedforms on tracer burial and movement (Hubbell & Sayre, 1964; Sayre & Hubbell, 1965).

Here, we present a flume study quantifying the effect of bed topography on tracer displacement in gravel-bedded rivers. We measured the displacement of 1,400 paramagnetic gravel tracers with different sizes at four different discharges in the Main Channel of the St. Anthony Falls Laboratory at the University of Minnesota. We also measured bed topography, water surface elevation, and total bedload transport rate. Mean bedform height, representing bedload sheets to dunes, varied from 2.5 to 4.4 cm over the different flows. Our goal was to document the effect on travel distance of bed forms and tracer particle size under different flows and bed-form dimensions.

The paper is structured as follows. In the following section, a brief review of the experimental setup is given. Section 3 describes the bed topography. Section 4 analyzes the statistics of tracer travel distances, and (a) examines the variation of travel distance with discharge and particle size, (b) estimates bedform trap efficiency based on the measured spatial distributions of tracer locations and the bed topography, (c) shows how the observed data are consistent with a theoretical model adopted from the extended active layer formulation (Wu, Singh, et al., 2019), and (d) provides a possible analytical form of tail characteristics of the travel distance distribution. Concluding remarks are given in Section 5.

2. Experimental Setup and Data Collection

We conducted experiments in the Main Channel facility at the St. Anthony Falls Laboratory, University of Minnesota. The Main Channel is 84 m long, 2.75 m wide and has a maximum depth of 1.8 m with a maximum discharge capacity 8,000 L/s. A 55 m long upstream section of the Main channel was used for this study. The Main Channel was operated as a water-feed, sediment recirculating system. Water is drawn directly from the Mississippi River and returned to the river after passing through the flume. Sediment is trapped through a slot in the bed and returned immediately to the upstream end via a slurry pump. The channel bed was composed

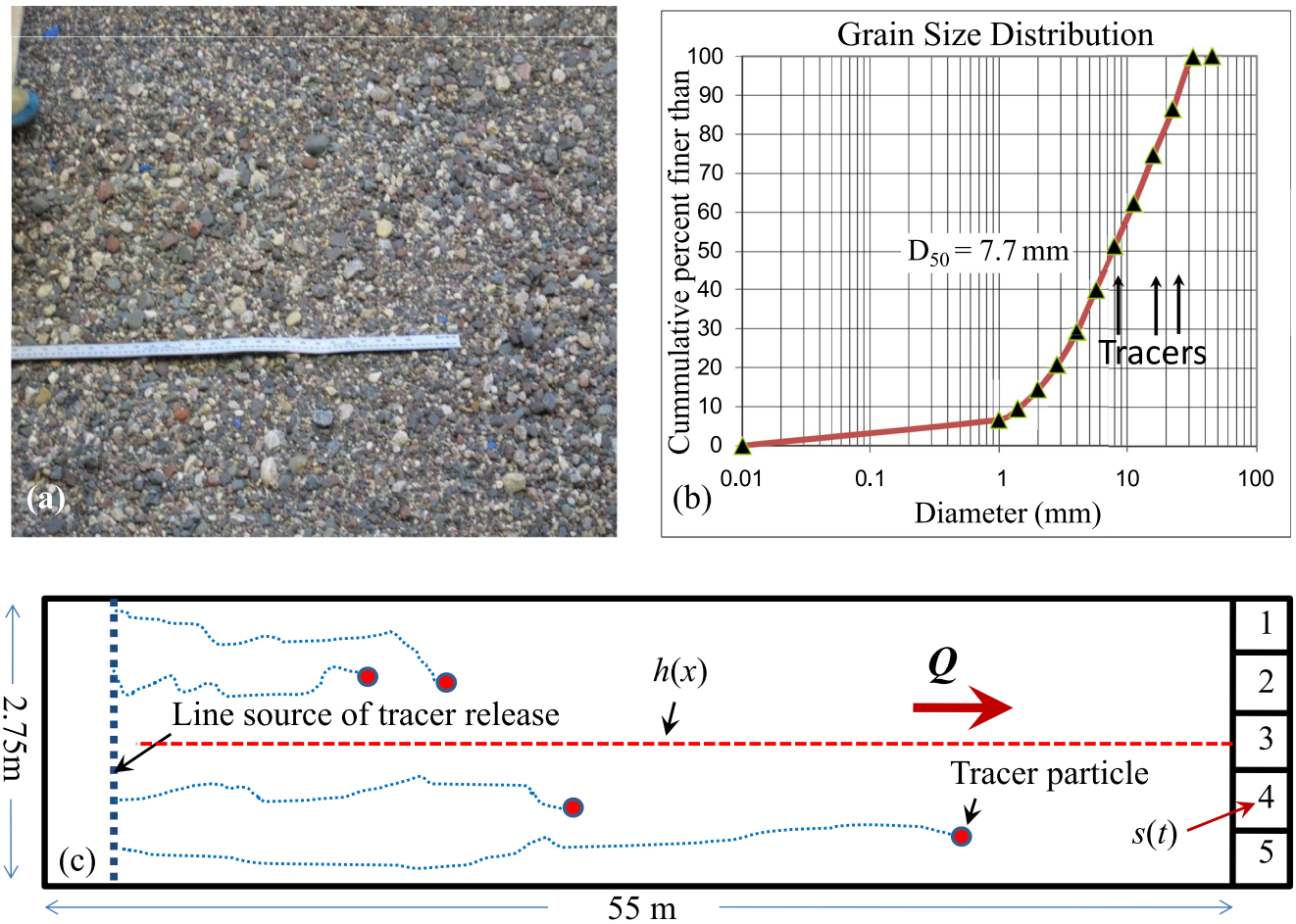

Figure 1. (a) A photograph of the water-worked bed showing the grains present on the surface for a discharge of 800 L/s, (b) grain size distribution of the initial bed material and, (c) schematic of the experimental setup showing the domain of measurements of bed elevation $h(x)$ and sediment flux $s(t)$. Examples of a few tracer particles with their trajectories are sketched. Water surface, bed elevations and sediment flux were measured for 5 hr after equilibrium conditions were attained, and the tracers were introduced at the last 5 min of each run before the flow was shut down.

of a mixture of gravel and sand with a median particle diameter, D_{50} = 7.7 mm, and with D_{16} = 2.2 mm and D_{84} = 21.2 mm (Figure 1).

Prior to data collection, a constant water discharge, Q, was fed into the channel to achieve steady state in transport and slope adjustment for both water and bed surface. Determination of the steady state was evaluated by checking the stability of the 60 min average total sediment flux $s(t)$ at the downstream end of the test section. More details about the experimental setup can be found in Singh, Fienberg, et al. (2009), Singh, Lanzoni, and Foufoula-Georgiou, (2009), and Singh et al. (2010).

The flow depth for all the experimental runs was between 0.2 and 0.5 m (see Table 1 for relevant hydraulic parameters). Three different sizes (~8, 16, and 22 mm) of paramagnetic particles (45% magnetite) with the same density as the bed material, each size a different color, were used as tracers. These tracer particles and their distributions were representative of the coarse half of the bed grain size distribution (GSD) (see Figure 1b). In other words, the number of tracer particles of certain size D_g was determined based on the initial GSD of the bed material.

After attaining equilibrium, experiments ran for approximately 5 hr. During the entire duration of the run, bed topography and water surface elevation were measured along the channel centerline using a three-axis positionable data acquisition (DAQ) carriage (see schematic in Figure 1). The DAQ carriage could automatically traverse the entire 55 × 2.74 m test section and position probes to within 1 mm in all three axes. The DAQ carriage was controlled by a backbone computer that also served as the master time clock for all data collection in the study. Sediment transport rates were measured continuously in five slots leading to tipping weigh pans, which returned the sediment to the upstream end of the test section via a slurry pump.

Table 1
Hydraulic Conditions and Spatial Bed Elevation Statistics

Q (L/s)	Depth (m)	Avg. WS	Hydraulic radius (h_R) (m)	τ^* (computed using WS)	Std ($h(t)$) (cm)	$<H_{bf}>$ (cm)	Std (H_{bf}) (cm)	$<L_{bf}>$ (m)	Std (L_{bf}) (m)
600	0.217	0.005	0.187	0.085	0.96	2.53	0.67	6.2	4.25
800	0.245	0.0053	0.208	0.102	1.37	3.17	1.26	4.88	2.19
950	0.27	0.005	0.226	0.105	1.86	3.91	1.55	3.46	1.36
1,600	0.365	0.0037	0.288	0.105	2.56	4.41	2.34	3.1	1.33

Note. The columns are respectively for water discharge Q (L/s), flow depth (m), average water surface slope (WS), hydraulic radius (m), Shields stress (τ^*), standard deviation of bed elevation series Std ($h(t)$) (cm), mean bedform height $<H_{bf}>$ (cm), standard deviation of bedform height Std (H_{bf}) (cm), mean bedform length $<L_{bf}>$(m), and standard deviation of bedform length Std(L_{bf}) (m).

After 5-hr of flume operation, marked paramagnetic tracer particles (1,400 overall: 200 large, 400 medium, and 800 small) were released as a line source (depicted as dotted vertical line in Figure 1c) at the upstream end of the channel. The flow in the channel was allowed to run for another 5 min; then the channel was immediately shut down and drained. Once the channel bed drained, the tracer particles that had not passed the full length of the channel were found in the channel bed via visual inspection and a handheld magnetometer. The location and the size of each tracer particle was noted. Most of the tracer particles lying on the bed surface were found visually and those trapped into the subsurface were excavated carefully by digging the surface.

The data presented here are the spatial bed elevation (10 mm resolution surface scans) at the end of the run using a range finding laser attached to the DAQ, and the travel distances of tracer particles. Four runs at different discharges were used to produce different values of bed shear stress. Bed shear stress is often characterized in terms of the dimensionless Shields stress, τ_b^*. For steady, uniform flow it may be approximated as

$$\tau_b^* = \frac{h_R S}{R D_{50}}, \tag{1}$$

where h_R and S are the hydraulic radius and channel slope, respectively, and $R = 1.65$ is the relative submerged density of silica.

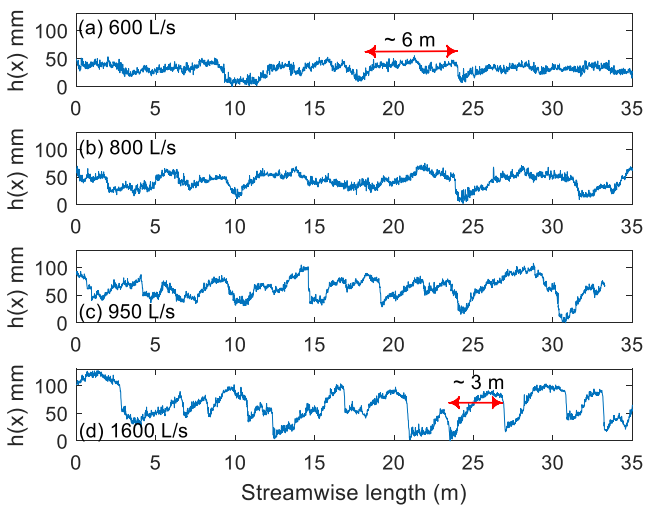

Figure 2. Longitudinal transects of bed profile elevations at a resolution of 10 mm (at the centerline of the flume) for the discharges of 600, 800, 950, and 1,600 L/s from top to bottom, with the average bedform lengths of 6.2, 4.88, 3.46, and 3.1 m, respectively. Notice that at low discharge of 600 L/s the bedforms are longer (average bedload sheets, ~6 m) whereas with increasing discharge the length of bedform L_{bf} decreases (e.g., ~3 m for 1,600 L/s) while bedform height H_{bf} increases.

Here we report the data collected at discharges of 600, 800, 950, and 1,600 L/s corresponding to average Shields stress of 0.085, 0.102, 0.105, and 0.105, respectively (Table 1) (Keylock et al., 2014; Ranjbar & Singh, 2020).

3. Characteristics of Bedform Geometry

Bed surface elevations were collected for all discharges following each experimental run (see Figure 1 for schematic and Figure 2 for the centerline transect of bed elevation) and the probability density functions (PDFs) of the mean-removed bed elevations were computed (Figure 3). As can be seen from Figure 3, the width of the PDF increases with increasing discharge, suggesting a wider range of bed elevations at higher discharges, which is also evident in the increasing standard deviation of bed elevations with increasing discharge (Table 1). Similar results of increasing standard deviation with increasing discharge were observed by Aberle and Nikora (2006); however, their experiments were conducted under armored bed conditions. Note that we did not observe bed armoring in any of our experiments since the bed was fully mobile (all grains on the bed surface in motion) and the migrating bedforms served to repeatedly remix the bed. In addition to the statistics, the PDF of the mean-removed bed elevation changes its shape from approximately unimodal (at low discharge) to bi-modal as discharge increases, suggesting that bedform dynamics (i.e., changing bedform geometry and kinematics) introduce additional bimodality to the bed elevation distributions (Figure 3).

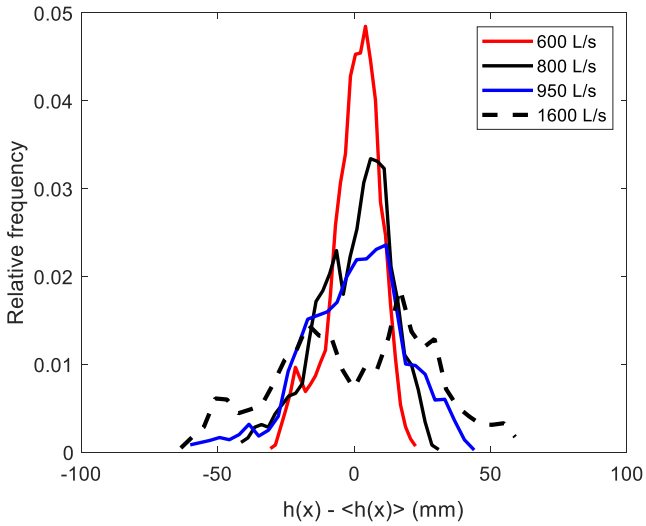

Figure 3. Probability density functions (PDFs) of the mean-removed bed elevation shown in Figure 2 for the discharges of 600, 800, 950, and 1,600 L/s. Notice the change of shape of the PDF from unimodal at low discharge to bimodal at high discharge.

Bedforms were extracted from the longitudinal spatial transects of bed elevation, using the methodology described in Singh et al. (2011). First, high-wavenumber fluctuations (i.e., smaller wavelengths, due to small scale bedforms or grain-scale variations) were filtered out using the Fourier transform of the spatial transect and then the signal was reconstructed with the remaining wavenumbers (corresponding to larger wavelength). After reconstruction, local maxima and minima of the filtered signal were determined and the differences between consecutive minima and maxima were computed. Finally, bedform height above a certain threshold (here, threshold = $2D_{50}$) was extracted. For more details, see Singh et al. (2011) and Singh, Guala, et al. (2012).

Bedform height increases and bedform length decreases with increasing discharge (Figure 2; Table 1). Average bedform heights for the discharges of 600, 800, 950, and 1,600 L/s were 2.53, 3.17, 3.91, and 4.41 cm, respectively. Average bedform lengths for the same discharges were 6.2, 4.88, 3.46, and 3.1 m. Notice that with increasing discharge both the mean and standard deviation of bedform height increases whereas the mean and standard deviation of bedform length decreases (Table 1). Bedforms were mainly bedload sheets at low discharge, transitioning to dunes with increasing discharge (Dinehart, 1992; Whiting et al., 1988).

The histograms of the bedform height H_{bf} and the bedform length L_{bf} for each discharge are shown in Figure 4. These distributions were obtained from the ensemble of bedform heights and lengths extracted from five longitudinal transects spaced 0.5 m apart, centered on the flume centerline. The ratio of mean bedform length L_{bf} to mean bedform height H_{bf} (aspect ratio) as a function of discharge (Figure 5) shows that the bedform aspect ratio decreases with increasing discharge, that is, bedform steepness increases with discharge, with the rate of decrease being faster for low discharge than for higher discharge.

4. Tracer Travel Distances

4.1. Tracer Travel Distances as a Function of Grain Size *D* and Discharge *Q*

To quantify the dynamics of individual particle motions, tracer particles were introduced at the upstream end of the channel (Figure 1c) for the last 5 minutes of each run. The mean travel distance for small, medium and large particles at discharges of 600, 800, 950, and 1,600 L/s (Figure 6) show that the distance for the largest tracer decreases with increasing discharge. For example, the mean travel distance for the large particles at a discharge of 600 L/s is ~24 m, whereas for the discharge of 1,600 L/s is ~8 m. An inverse relationship between discharge and mean travel distance is also observed for medium particles.

The inverse relationship between discharge and mean travel distance can be mainly attributed to the control by bedforms. Although increasing discharge increases the driving force for bedload motion, it also increases bedform height and steepness (Figures 2 and 5). Larger particles move by rolling and sliding and their travel distance over a planar bed is driven by fluid forces. If bedforms become large enough, the competition between increasing mobility (due to increasing driving force of higher discharge) and increasing bedform trap efficiency (fraction of grains trapped by a bedform; detailed discussions presented in Section 4.2), can tip toward bedform trapping. In the case of higher discharge (taller bedforms), most tracer particles were found buried in the lee face of bedforms. This observation is consistent with the observation of Foley (1977) that pebbles and cobbles were found buried under the bed layers during the process of scour and fill.

As a comparison, the short travel distances of the small size particles in Figure 6 suggest that small particles, in general, can stop motion more easily. That said, their mean travel distance almost doubles (from ~3 to ~ 6 m) as discharge increases from 600 to 1,600 L/s. This implies that the increasing mobility of small particles plays relatively a more important role than the trap efficiency of bedforms as the discharge increases, which may be related to their motion by saltation at high discharges. As a result, smaller particles at higher discharge are not as easily trapped and can move further. At the highest discharge of 1,600 L/s, the mean travel distance is nearly

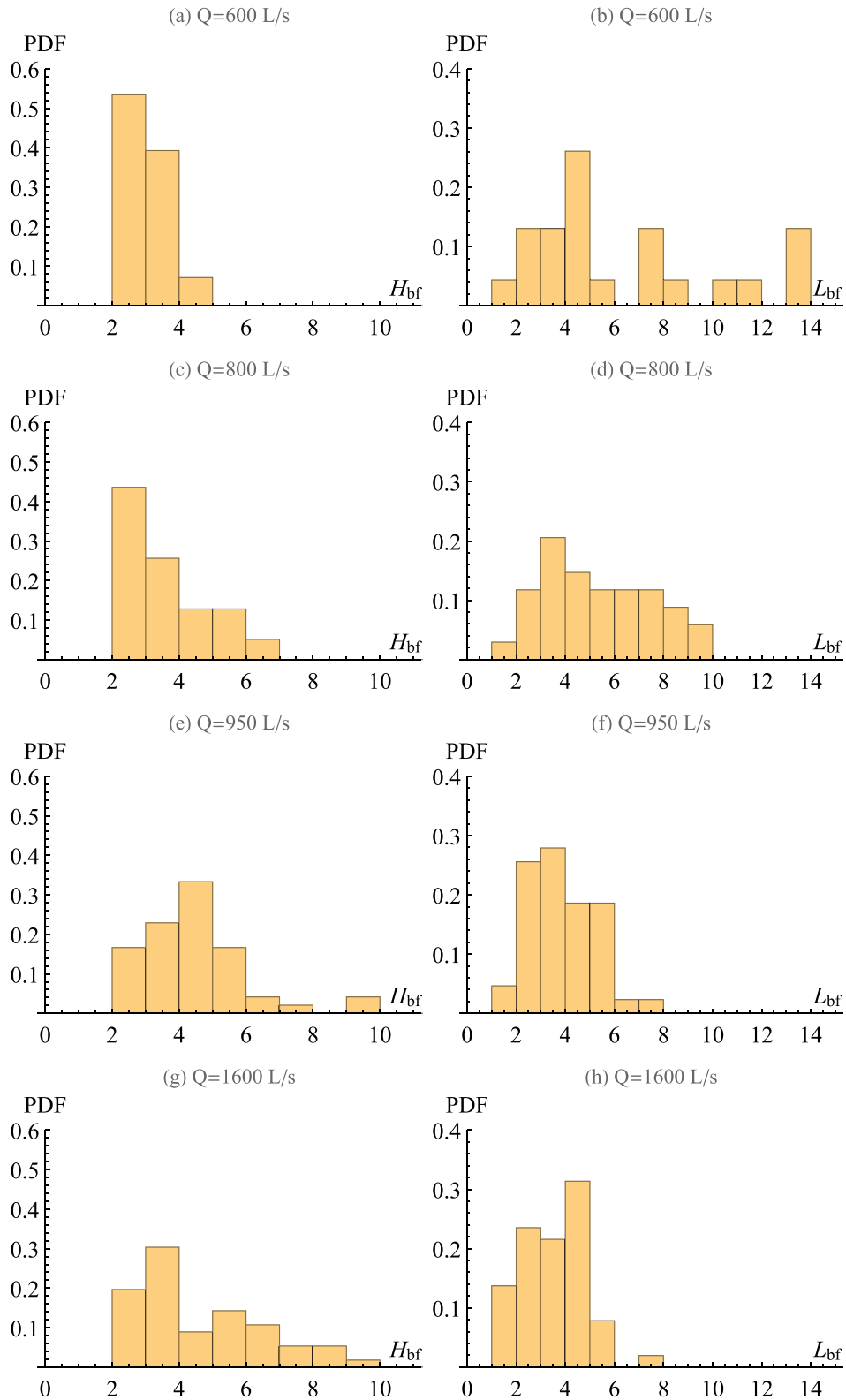

Figure 4. PDFs of bedform height (H_{bf}, left column) and bedform length (L_{bf}, right column) obtained from five alongstream transects of bed elevation with 0.5 m spacing, centered on the flume centerline, at the end of each run (see Section 3 for bedform extraction). The x-axis in subplots indicates H_{bf} (left column, cm) and L_{bf} (right column, m).

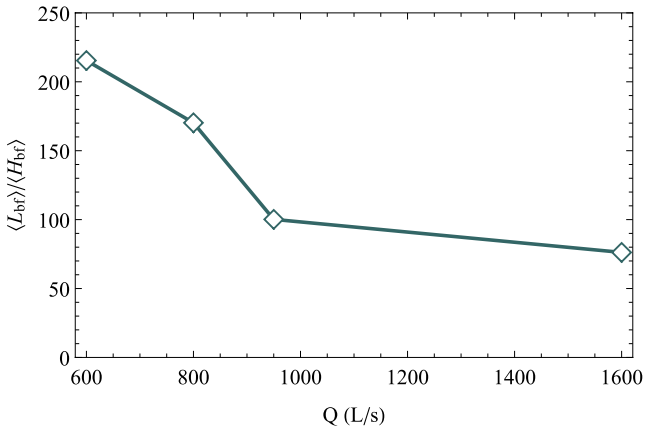

Figure 5. Aspect ratio ($<L_{bf}>/<H_{bf}>$) as a function of discharge. Notice that with increasing discharge the aspect ratio decreases.

the same for all tracer sizes, suggesting that bedform trapping controls the streamwise travel of all bedload particles. The standard deviation of the travel distances follows the same pattern as the mean travel distances, decreasing with increasing discharge for both large (Figure 6b) and medium (Figure 6c) particles, whereas it does not change significantly with discharge for smaller (Figure 6d) particles.

The cumulative density functions (CDFs) of tracer travel distances for all discharges (Figure 7) show that while for the lowest discharge (600 L/s), the CDF of small size tracer particles is quite distinct from the CDFs of medium and large particles, for the highest discharge (1,600 L/s) the CDFs of all three size tracer particles almost collapse. For example, at 600 L/s approximately 88% of large particles, 66% of medium particle and 5% of small particles travel further than the average bedform length of ~6 m, indicating that small tracer particles were mostly trapped in the first bedform, whereas the larger grains can skip over one or more bedforms (Figure 7a). In contrast, at 1,600 L/s, 25% large, 23% medium and 22% small particles travel further than the same length of ~6 m (about twice of the average bedform length at 1,600 L/s, ~3 m), which suggests that nearly all grains of all sizes were trapped in the first couple of bedforms. On the other hand, the similarity of the small particle CDFs at high and low discharges agrees with our interpretation that the small particles generally stop motion more easily. That said, the reasons for the observed similar

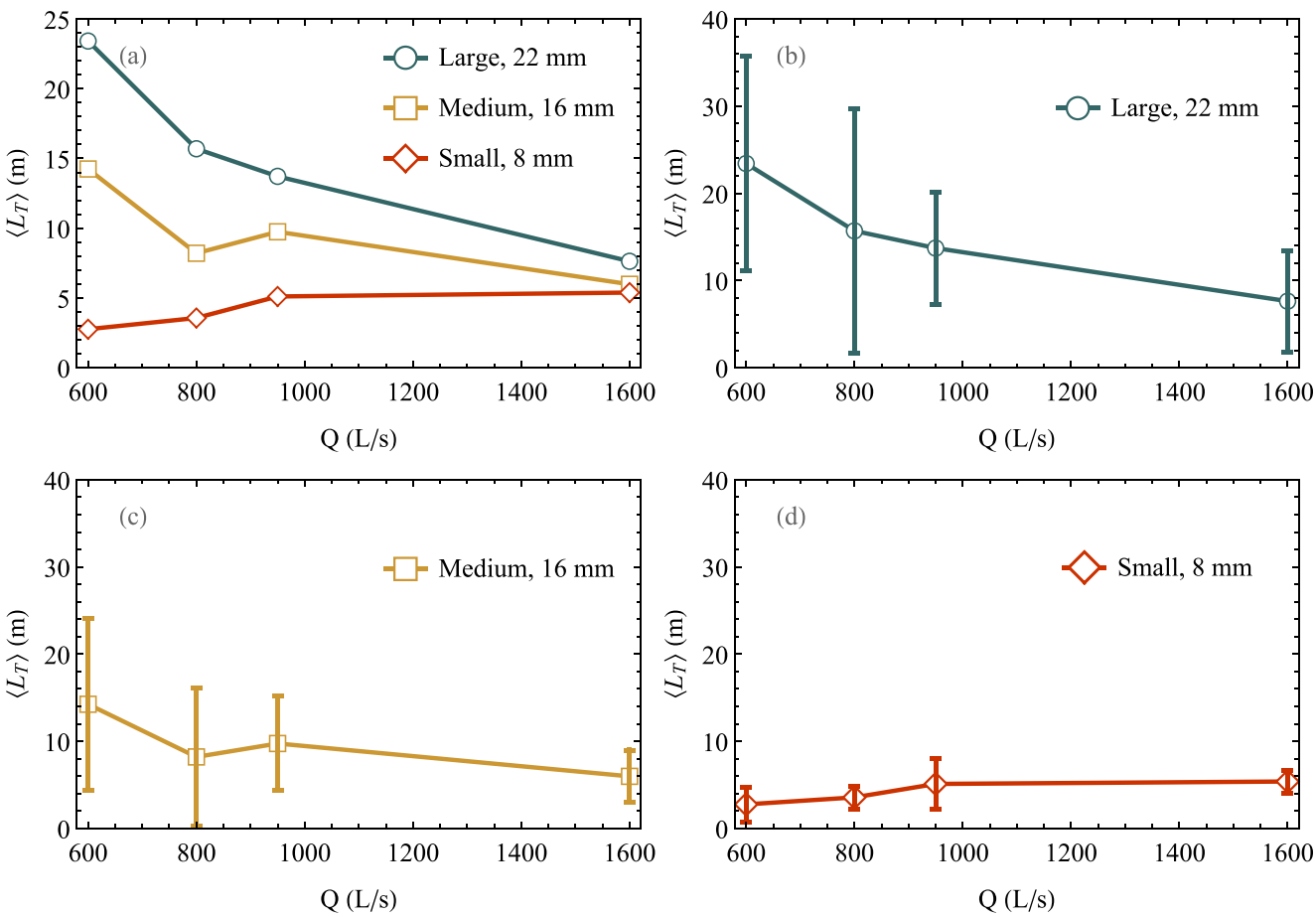

Figure 6. (a) Mean travel distances of the large (22 mm), medium (16 mm), and small (8 mm) tracer particles as a function of discharge. Error bars in (b), (c), and (d) represent the standard deviation of travel distances for the large, medium and small tracer particles as a function of discharge, respectively. Mean travel distance decreases with discharge for the largest two tracer classes. The standard deviation of travel distance also decreases with discharge for the large and medium particles, whereas the standard deviation does not change significantly for the small particles.

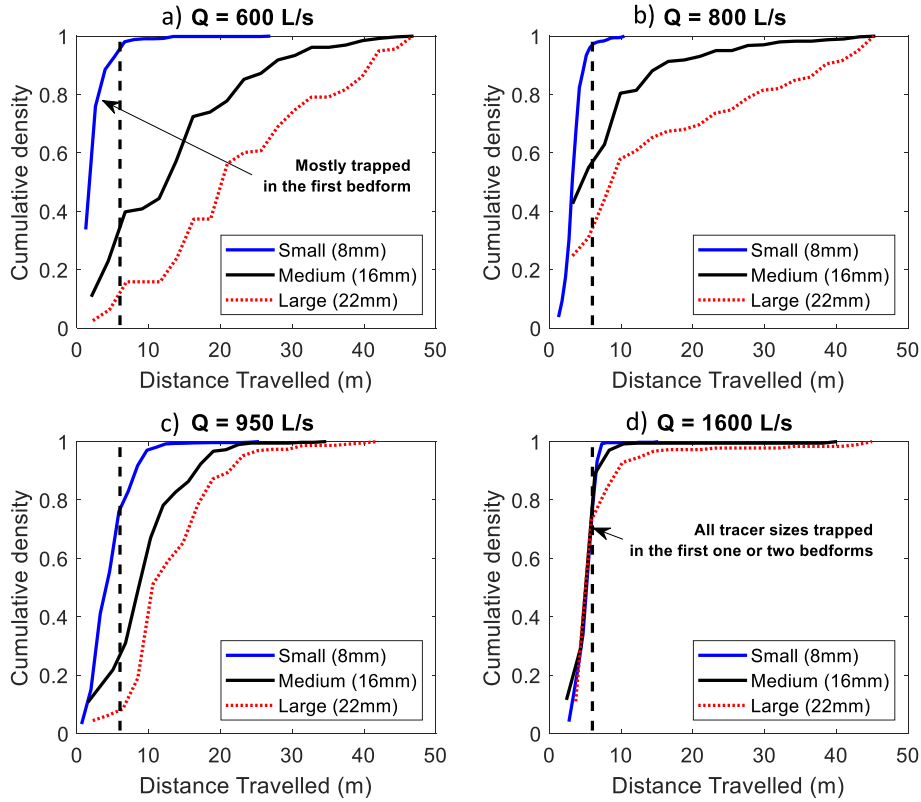

Figure 7. Cumulative density functions of tracer travel distances for the discharges of 600 L/s (a), 800 L/s (b), 950 L/s (c), and 1,600 L/s (d). Vertical dashed lines indicate the average bedform length for the discharge of 600 L/s (~6 m).

CDFs of small tracers may be different: on "plane bed" (small bedforms as in Figure 2a under the discharge of 600 L/s), trapping may occur because the grains can more easily lodge in small sheltered spots on the bed; while with larger bedforms at higher discharges, the small particles may stop primarily due to the increase of the trap efficiency of the bedforms.

4.2. Trap Efficiency of Bedforms for the Downstream Transport of Tracer Particles

To further investigate the spatial dependence of tracer location and bed configuration, we superimposed the particle locations on the bed topography, both of which were captured at the end of each experiment (Figure 8). The location and the spatial pattern of tracers and bedforms suggest that the bed configuration plays a dominant role in determining the deposition location of most tracers. At the same time, some tracers clearly passed over one or more bedforms before becoming trapped. This leads us to consider a model in which tracer travel distance is probabilistically determined by the trap efficiency of the bedforms (see also, Pyrce and Ashmore (2005) and Hassan and Bradley (2017)).

Specifically, we explore a model in which the trap efficiency depends on the size of the tracer grain D_i relative to the height of the bedform H_{bf}, using not only the final position of each tracer relative to the bedform on which it stopped, but the full record of tracer-bedform *encounters* for each tracer grain to incorporate spatial bed configuration. For example, if a tracer grain passed over two bedforms and became trapped on a third, the data set would include two instances of bedform passing and one of trapping.

To build the data set for grain trapping and passing, we first designated the bedform on which a grain was found as that which trapped the grain, recording the tracer grain size and bedform height. For this purpose, the domain of a bedform was extended downstream of its lee slope by a distance of $5H_{bf}$. In a few cases, the tracer was located on a plane bed (elevation variation less than 1.5 cm) and could not be associated with any bedform. These grains did not contribute to the trapping data set. For the passing data set, we recorded all bedforms upstream of the

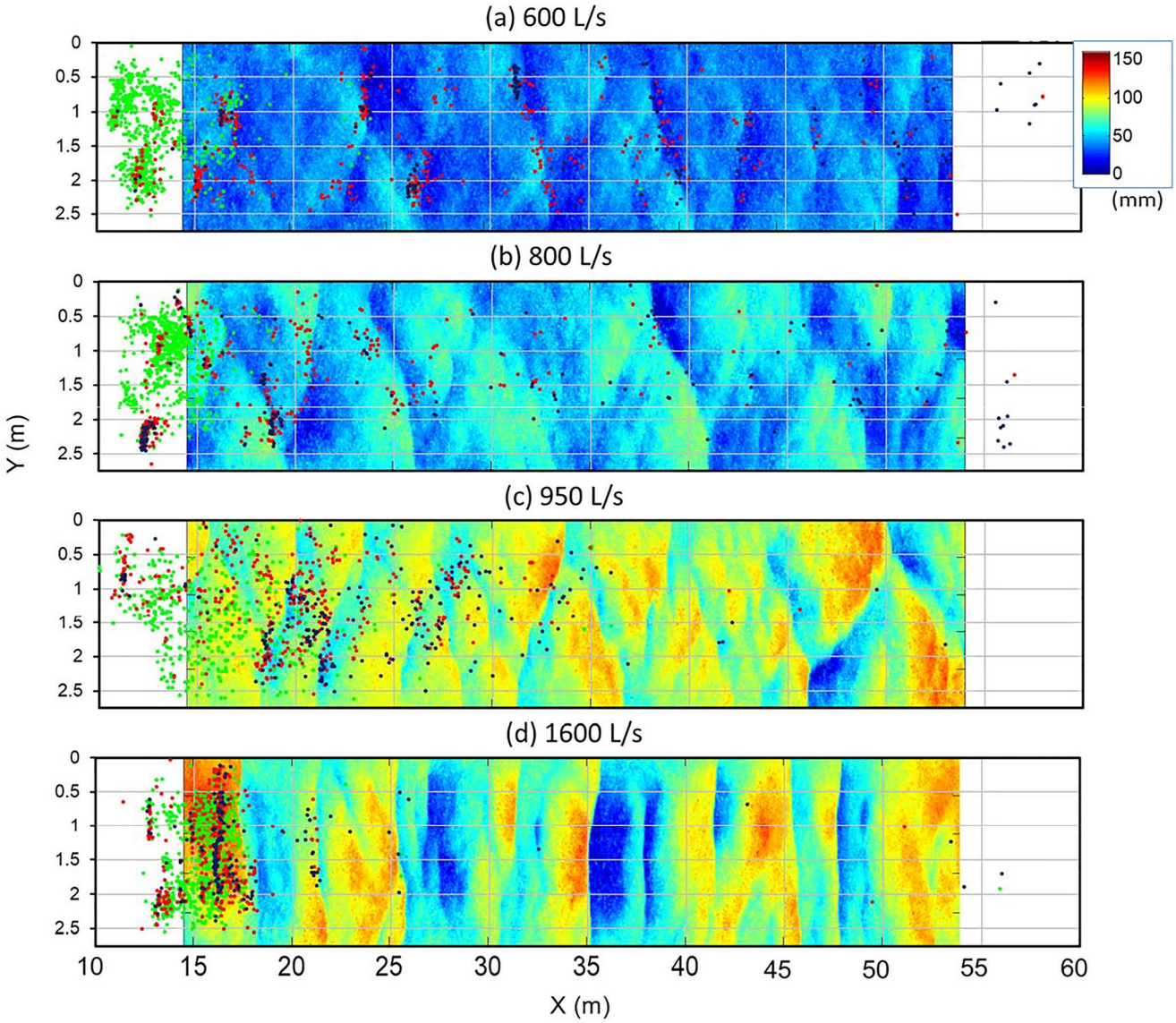

Figure 8. Map of tracer location and bed topography under different discharges of (a) 600 L/s, (b) 800 L/s, (c) 950 L/s, and (d) 1,600 L/s. Data collected from drained bed after each run. Green, Red and Blue dots represent small, medium and large tracer particles, respectively.

trapping bedform using a straight-line path at the lateral position of the tracer. These bedforms were noted as passing encounters and the tracer grain size and bedform height for each encounter was recorded.

We can identify two sources of error in our method of recording tracer–bedform encounters. In some cases, a tracer may have been traversing a bedform when the five-minute tracer experiment ended and the flow was turned off. If trap efficiency does, in fact, increase with H_{bf}/D_i, this error might record trapping on smaller bedforms that would not, in reality, trap the grains. A second possible error arises from using a straight-line path to identify those bedforms that a tracer has passed over. In the presence of lateral variability in bedform height and crest orientation, passing grains may, in fact, follow a sinuous path, passing through low places on the bedform. If trap efficiency increases with H_{bf}/D_i, this error might record bedform passing for larger H_{bf} than actually recorded.

According to the above description, we calculated the bedform trap efficiency E_{tr} as a function of the ratio of bedform height to grain size H_{bf}/D_i:

$$E_{tr} = \frac{N_{tr}}{N_{tr} + N_p}, \tag{2}$$

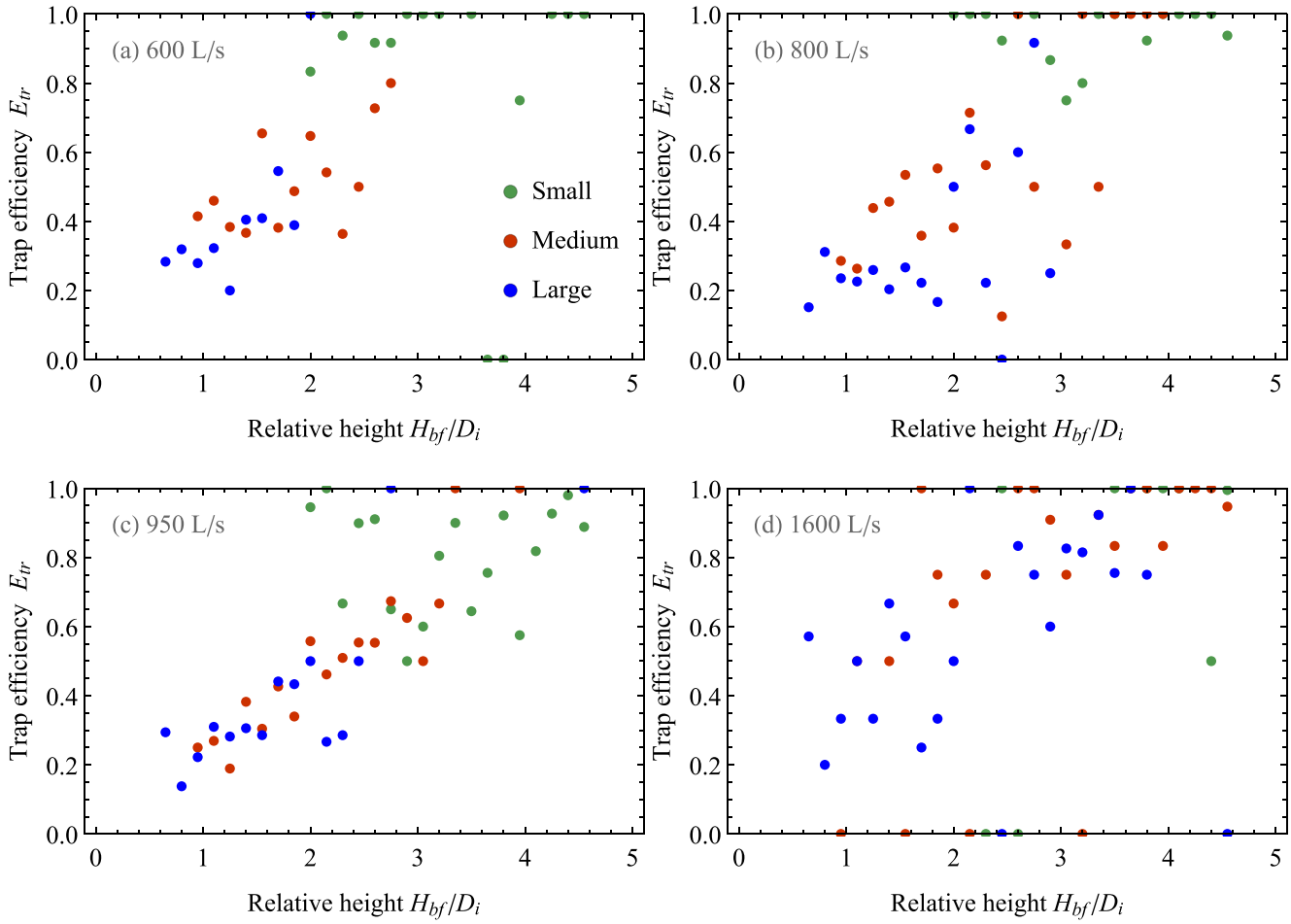

Figure 9. Calculated bedform trap efficiency as a function of the ratio of bedform height to grain size H_{bf}/D_i. Trap efficiency observations are grouped into bins of 0.15 in H_{bf}/D_i.

the results of which are displayed in Figure 9. In the above equation N_{tr} is the number of particles trapped by the bedform, and N_p is the number of particles that passed a bedform. Note that all terms in Equation 2 are a function of H_{bf}/D_i. Minimum values of H_{bf}/D_i for tracer particles of different sizes are defined by the minimum threshold, 1.5 cm, for defining a bed form, which corresponds to H_{bf}/D_i of ~2, ~1, and ~0.7 for small (8 mm), medium (16 mm), and large (22 mm) tracer particles.

Generally, the results indicate that relative bedform height H_{bf}/D_i dominates travel distance of particles for all sizes and all flows (Figure 9). At a discharge of 600 L/s, small tracer particles are trapped by bedforms with relative height between 2 and 3 with high trap efficiencies (>80%). As discharge increases to 950 L/s (Figure 9c), trap efficiency for small tracers decreases, suggesting that some small tracers can skip over bedforms via saltating or lateral excursions to low points on bedforms. However, at 1,600 L/s, trap efficiency for small tracers increases back to one and nearly all are trapped in the first (very large) bedform. For medium and large tracers, trap efficiency at 800 L/s is more scattered and smaller than for the smallest flow, suggesting that increased flow strength and the availability of broad low bed form passes may contribute to bedform passing (Figure 8). As flow increases to 950 L/s, bedforms steepen and more consistently trap medium and large grains.

The overall trend between trap efficiency and H_{bf}/D_i is similar over grain sizes, suggesting a common relation (Figure 10). Large particles (blue dots) show slightly lower trap efficiency than medium particles (red dots) for H_{bf}/D_i up to ~2.3. Small particles (green dots) show higher trap efficiency in the range of H_{bf}/D_i between 2 and 3, with the lower limit $H_{bf}/D_i \sim 2$ discussed above. Setting aside these differences, combining all particle sizes (black circles) and discharges indicates a linear relationship between trap efficiency and H_{bf}/D_i (with a slope change at an approximate scale of $H_{bf}/D_i \sim 3.7$). An approximately linear increase in trap efficiency with relative

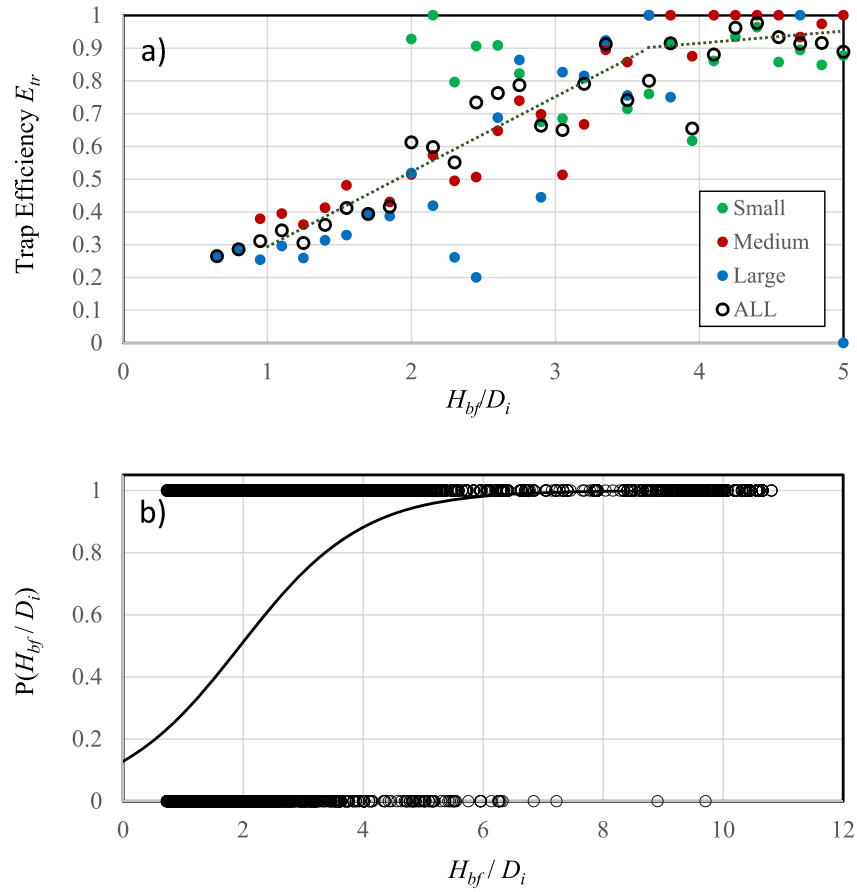

Figure 10. (a) Trap efficiency for particles of each size based on results combining all flows. (b): Trapping probability obtained from a logistic fit to tracers combining all sizes and flows. The black circles in (b) represent either trapped particles (i.e., $P(H_{bf}/D_i) = 1$) or passed particles (i.e., $P(H_{bf}/D_i) = 0$). The dashed line in (a) provides a suggestive relation (guideline) between trap efficiency and relative bedform height.

bedform height is consistent with direct observations that higher bedforms are more efficient in trapping grains. In addition, this relationship indicates an approximate 50% trap efficiency at $H_{bf}/D_i = \sim 2$, 90% trap efficiency at $H_{bf}/D_i = \sim 4$, and a possible lower limit to trap efficiency of ~25%. A similar result is achieved when fitting a logistic function ($P(x) = \frac{1}{1+e^{-k(x-x_0)}}$, where $k = 0.98$, $x_0 = 1.95$ are the fitted model parameters and $x = H_{bf}/D_i$), as a standardized way to combine observations of trap or pass, to the trapping/passing observations as a function of H_{bf}/D_i for all flows and all tracer sizes (Figure 10b). For example, it can be seen from Figure 10 that trap efficiency (Figure 10a) and logistic fit (Figure 10b) for all flows and all tracer sizes are quite similar: both centered on 50% trapped at $H_{bf}/D_i = 2$ and have 90% trapped at $H_{bf}/D_i = 4$. Note that a poor logistic fit for small tracers (most were trapped) was obtained whereas the logistic fits improves with increasing particle size (not shown for brevity).

Table 2
Trap Efficiency of Each Tracer Size at the Mean Bedform Height

		Small		Medium		Large	
Q (L/s)	$<H_{bf}>$ (cm)	$<H_{bf}>/D_i$	E_{tr} @ $<H_{bf}>$	$<H_{bf}>/D_i$	E_{tr} @ $<H_{bf}>$	$<H_{bf}>/D_i$	E_{tr} @ $<H_{bf}>$
600	2.53	3.16	1	1.58	0.47	1.15	0.33
800	3.17	3.96	1	1.98	0.44	1.44	0.28
950	3.91	4.89	0.82	2.44	0.53	1.78	0.34
1,600	4.41	5.51	1	2.76	0.72	2.00	0.54

Note. E_{tr} @ $<H_{bf}>$ represents trap efficiency at mean bedform height interpolated from trap efficiency versus $<H_{bf}>/D_i$ plots (see Figure 9) for each particle size and discharge.

To further generalize tracer behavior across grain sizes and flows/bedform heights, we examine mean trap efficiency for each tracer size using mean bedform height $<H_{bf}>$ for each run. We have previously observed the competition between the effects of driving force (shear stress) and bedforms on the particle travel distance as the discharge increases, indicating that increasing discharge can increase the shear stress and thus increase the travel distance, while at the same time the increasing discharge can also increase bedform height and thereby decrease the travel distance. From Table 2, we demonstrate

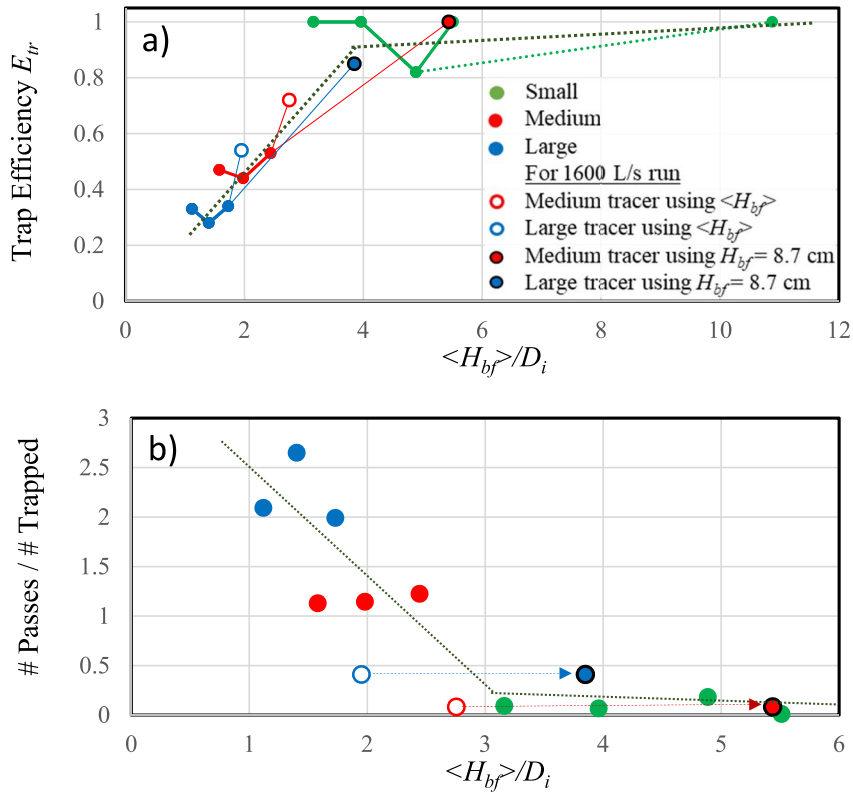

Figure 11. Tracer trap efficiency as function of $<H_{bf}>/D_i$. (a) Trap efficiency for each tracer size; (b) fraction of grains passing bedforms. For flow of 1,600 L/s, values using $<H_{bf}>$ are shown with an open symbol and values using H_{bf} = 8.7 cm are shown with a black boundary. 8.7 cm is the height of the upstream bedform at that discharge, which trapped almost all grains encountered. The dashed lines indicate approximate relation (guidelines) between trap efficiency and relative bedform height. Dashed arrows in (b) link the two values of H_{bf} at 1,600 L/s.

that as the driving force and bedform height increase, trap efficiency increases, similar to plots of E_{tr} versus H_{bf}/D_i for each grain size and run (Figure 9). This suggests that the increase in trap efficiency with increasing bedform height dominates the effect of stress on travel distance. The effect of mean bedform height on trap efficiency is also illustrated in Figure 11, showing a common trend across grain sizes. For a flow of 1,600 L/s, $<H_{bf}>$ = 4.41 cm, whereas almost all tracers were trapped in the first bedform encountered, which had H_{bf} = 8.7 cm (Figure 8). To provide a more representative illustration, trap efficiency is plotted for both $<H_{bf}>$ and H_{bf} = 8.7 cm in Figure 11. Overall, the trap efficiency increases consistently with relative bedform height (Figure 11a) and the fraction of passing grains drops to nearly zero as relative bedform height approaches 3 (Figure 11b).

4.3. Tracer Transport Model Based on the Extended Active Layer Formulation for the Observed Travel Distances

Here, we hypothesize a theoretical model and check its validity for the experimentally measured travel distances of the tracer particles. Theoretical explorations regarding the transport of tracer bedload particles have mainly focused on the idealized case of uniform particle size and equilibrium transport conditions, typical examples of which are the studies based on the active layer formulation (e.g., Ganti et al. (2010); Lisle et al. (1998)) and its extensions (Pelosi et al., 2016; Wu, Foufoula-Georgiou, et al., 2019; Wu, Singh, et al., 2019). Although idealized, analytical results from such studies have demonstrated their ability to capture important characteristics of bedload particle movement in real river systems (Wu, Foufoula-Georgiou, et al., 2019; Wu, Singh, et al., 2019), where wide distributions of particle sizes and flow discharges exist and can impact the transport processes.

In the work of Wu, Singh, et al. (2019), a fluctuating riverbed surface is chosen as the streamwise reference system and the classic active layer formulation is extended and shown to effectively account for the presence and dynamics of bedforms. Specifically, a tracer particle is considered to move vertically downward into the riverbed if it is buried by other particles arriving from upstream, whereas a buried tracer particle moves upward relative to

the bed surface when particles above it are entrained, until it eventually reaches the surface and can travel downstream. This vertical motion (up and down in the bed) was shown to follow a random-walk process and governed by a diffusion equation, which is coupled with an advection-diffusion equation (ADE) for the streamwise transport of particles on the bed surface (Wu, Singh, et al., 2019).

One of the important conclusions of Wu, Singh, et al. (2019) was the existence of the normal diffusion regime for the streamwise bedload tracer transport at both small- and large-timescales. The large timescale corresponds to a characteristic time at which the tracers have mixed uniformly across the depth of the riverbed due to fluctuations of the bed surface (and thus up and down motions of the tracers). For the experiments considered in the present study, the 5 min transport period is not likely sufficient for full vertical mixing of the tracer particles, such that the transport regime for the tracers should be close to that for the small timescale process (Wu, Singh, et al., 2019). Note that the smallest timescales in Wu, Singh, et al. (2019) model are still larger than those for the ballistic regime related to the inertial effect of the particle (Nikora et al., 2002). The normal diffusion regime implies that tracer transport can be described by an ADE, as indicated by Wu, Singh, et al. (2019):

$$\frac{\partial C}{\partial t} = -c\frac{\partial C}{\partial x} + D_x\frac{\partial C^2}{\partial x^2}, \tag{3}$$

where C is the PDF of the streamwise location of the tracer particle, t is time, c the virtual velocity, x the streamwise coordinate, and D_x the streamwise diffusion coefficient (see for details, Wu, Singh, et al., 2019).

With the initial condition of releasing the tracer particles instantaneously as a line source at the upstream end of the channel, the analytical solution of Equation 3 can be obtained as

$$C(x,t) = \frac{1}{\sqrt{4\pi D_x t}}\left\{\exp\left[-\frac{(-x-ct)^2}{4D_x t}\right] + \exp\left[-\frac{(x-ct)^2}{4D_x t}\right]\right\}. \tag{4}$$

Since we have the statistics for tracer travel distance L_T, we can determine the virtual velocity c and diffusion coefficient D_x by the following relations (Wu, Singh, et al., 2019):

$$\langle L_T \rangle = ct \tag{5}$$

and

$$\sigma^2(t) = 2D_x t, \tag{6}$$

where $\sigma^2(t)$ is the variance of travel distances at a given time t. Note that observation periods for tracer movements were the same for all experimental runs, that is, $t = 5$ min or 300s.

Based on Wu, Singh, et al. (2019), the streamwise distribution of the tracer particles as given by Equation 4 can be interpreted as an ensemble average corresponding to several realizations of experimental measurements with different bedform configurations for different runs with the same transport condition. Hence, it may be used to estimate how far a particle can travel downstream, on average, in the presence of bedforms. In this case, we can directly compare the model result of Equation 4 to the measured streamwise distribution of tracer particles without considering the specific bed topography, which can thus be applied to places where topographic data are not available (e.g., the first 5 m from the location of introduction of tracers in the current study).

Comparison of observed travel distances with theoretical predictions of Equation 4 is shown in Figure 12. It is seen that for relatively low discharges and small particles, the Gaussian distribution of Equation 4 largely captures the body of PDFs of measured travel distances, providing experimental evidence of the normal diffusion of bedload particles at small timescales as proposed by Wu, Singh, et al. (2019).

We note that as the initial condition of the tracer transport, tracer particles were introduced to the flow by releasing them through the water column. Thus, tracers were in motion when introduced to the flume. Most of the tracers were then observed to perform only a couple of steps during the next 5 min experimental interval, which indicates that waiting times of particles do not come into play for the transport process. Again, we emphasize that the model result of Equation 4 may predict how long a distance a particle can travel downstream based on the ensemble average strength (i.e., size) of bedforms. Thus, if there is no preferential trapping (i.e., unusually high trapping of the tracer grains relative to the model predictions by an uncommon high bedform), in a specific realization of the bed configuration, the travel distances for tracer particles should result in a "normal distribution"

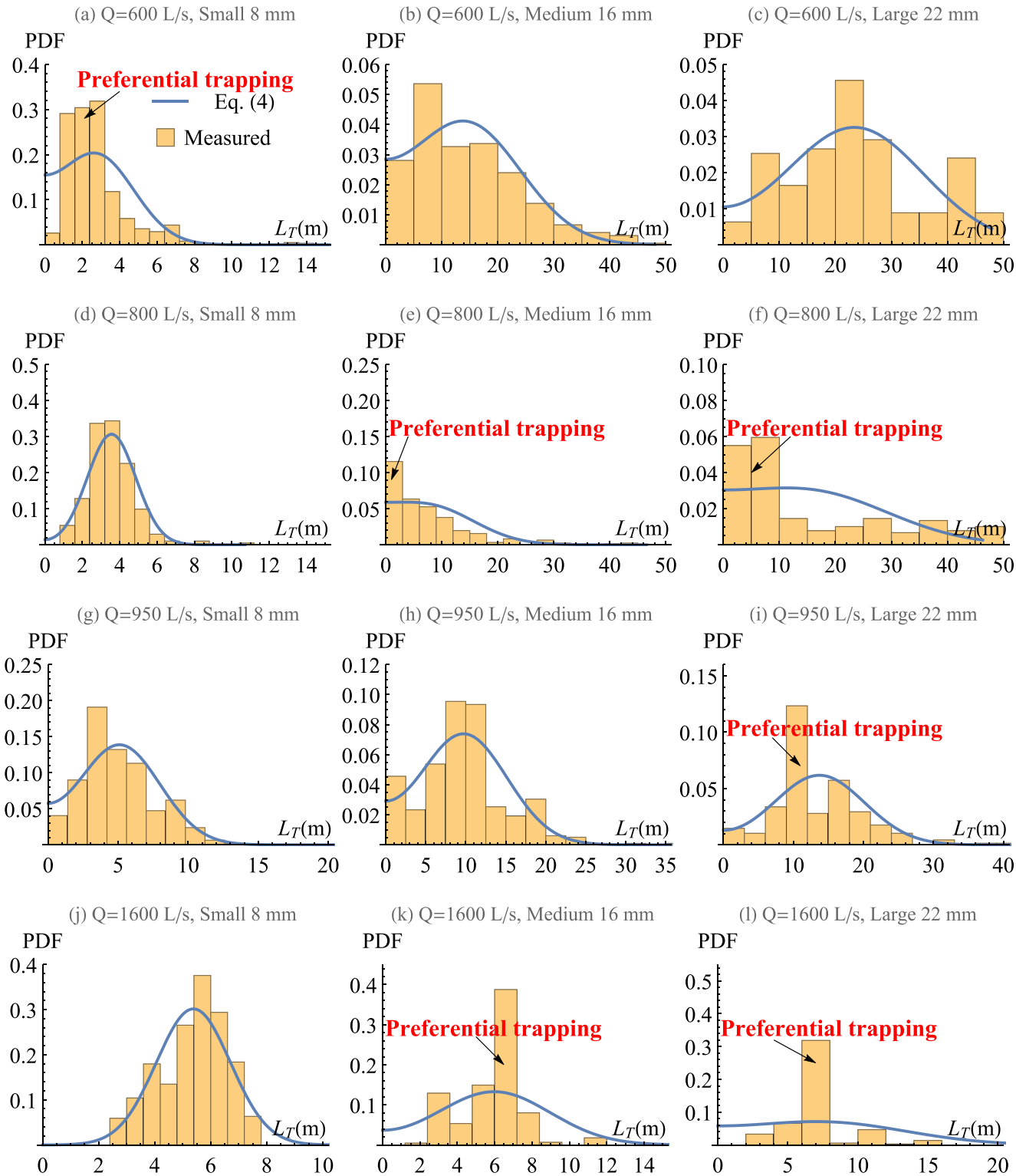

Figure 12. Comparison of tracer travel distance (L_T) PDFs between theoretical predictions of Equation 4 (blue lines) and the experimental measurements (yellow bars). Other than cases with strong "preferential trapping" (roughly determined as an approximately 100% or greater deviation of the measurements from the theoretical predictions, as illustrated in subfigures *a*, *e*, *f*, *i*, *k*, and *l*), where a large amount of particles were trapped in by individual or a couple of bedforms, the Gaussian distributions of Equation 4 (in particular, truncated Gaussian) can largely capture the body of the PDFs. The width of the yellow bars (i.e., bin size) in each subfigure is chosen in such a way that the number of bins is the same under the area by the blue line of Equation 4, that is, we use the same number of bars to characterize the tracer plume in each subfigure. Note that the discrepancy observed between the measured and predicted PDFs of travel distances highlights the nature of preferential trapping.

of the tracer plume as predicted by Equation 4. This provides a reference for evaluating the influence of bedform trapping strength on travel distance based on differences between the theoretical predictions and the experimental measurements. On Figure 12, we indicate instances of "preferential trapping" by identifying spots with almost 100% or greater deviation of the experimental measurements from the theoretical predictions of Equation 4.

Focusing on the tracer travel distance PDFs for the small particles (left column in Figure 12), it can be seen that as the discharge increases, the particles generally travel longer distances in terms of the mean travel distance as observed in Figure 6a compared to larger particles. Considering the average bedform length of ∼6 m for the discharge of 600 L/s, from Figure 12a we can infer that most of the tracers may have been trapped in the first bedform, thus any spatial heterogeneity in this individual bedform may play a major role in trapping the particles. Additionally, differences between the theoretical and experimental results suggest a "preferential trapping" over the streamwise locations from 1 to 3 m. The relative frequency of the highest bin in Figure 12a is close to 0.4, which is almost a 100% deviation from the amount of tracers that may "normally" be trapped (the theoretical prediction of Equation 4 around the same streamwise location gives a value of ∼0.2), suggesting remarkable bedform structures in this area. "Preferential trapping" as used here indicates that bedform trapping is variable, depending on local factors such as bedform shape and orientation that may provide larger trap efficiency. Given the lower relief bedforms at 600 L/s, behavior of the larger particles approaches that of the "plane bed," which is supported by results in Figures 12b and 12c, illustrating relatively good agreement between theoretical and experimental results.

Figure 12j demonstrates that the majority of small particles may have traveled through a couple of bedforms at the discharge of 1,600 L/s (mean travel distance of ∼6 m with the majority distributed in the range [2, 8] m, compared with the mean bedform length of ∼3 m). It is observed that these small tracers are relatively normally distributed, although two small spikes can be noticed around the streamwise locations of ∼3 and ∼6 m. This may suggest, again, the locations of pronounced bedform structures, which can be supported by the "preferential trapping" observed for both medium and large particles in Figures 12k and 12l. We emphasize again that the application of the active layer formulation has demonstrated that a simple transport model can roughly capture the bedload tracer transport process in more complex conditions (specifically, we have tested the hypothesis of normal diffusion of tracers at small timescales). On the other hand, the active layer formulation provides a reference for evaluating the influence of bedform trapping strength on travel distance (identified as "preferential trapping") based on differences between the theoretical predictions of this model and the experimental measurements.

4.4. Pdfs of Tracer Travel Distances: Implication for Tail Characteristics of Step Length Distribution

Sediment in real rivers is subjected to a range of discharges, from low flows to large floods. Tracer particles in real rivers experience a variety of bed configurations, ranging from plane bed conditions to bedform-dominated conditions. The overall (size-independent) distribution of the particle travel distances in that case will be a mixture of the individual size-dependent particle travel distance PDFs at different discharges. Ganti et al. (2010) proposed a framework in which the convolution/mixture of the PDFs of step lengths for individual particles results in a power-law distribution (see also Meerschaert and Scheffler (2001)). In particular, they showed that the convolution of the thin-tailed distributions of step lengths of size-dependent particles with the thin-tailed PDF of the particle sizes leads to a heavy-tailed distribution. Similar results were shown by Hill et al. (2010), who argued that a power-law PDF of travel distances can emerge from superposition of exponential PDFs of travel distances of grains of different sizes D, where the PDF of D is thin tailed. To evaluate the effect of variable discharge on the PDF of travel distances in our experiments, we combine the results into two groups in order to simulate the combined effect of low and high transport rates. The runs with smaller bedforms (600 L/s, $<H_{bf}> = 2.5$ cm and 800 L/s, $<H_{bf}> = 3.2$ cm) are combined, as are the runs with larger, steeper bedforms (950 L/s, $<H_{bf}> = 3.9$ cm and 1,600 L/s, $<H_{bf}> = 4.4$ cm).

Before we move on to the results, attention should be paid to the definitions of step lengths and travel distances. While the former refers to the distance traveled continuously by a tracer from the start to the end of its motion (Furbish et al., 2012; Wu et al., 2020), the latter considers the total distance traveled during an observation period. That is, during a given period (e.g., the 5 min duration of tracer transport in our experiments), a tracer may perform multiple steps resulting in an excursion punctuated by various waiting times. We did not track the trajectories of each tracer during the experiments, so a determination of step length distribution is not possible. The travel distances of the tracers can still provide some information on the possible form of the step length distribution, especially given that we rarely observed tracers performing more than one step over the 5-min duration of the experiments. However, understanding differences between the two variables will be helpful in explaining some of the results regarding the tail characteristics of the distributions.

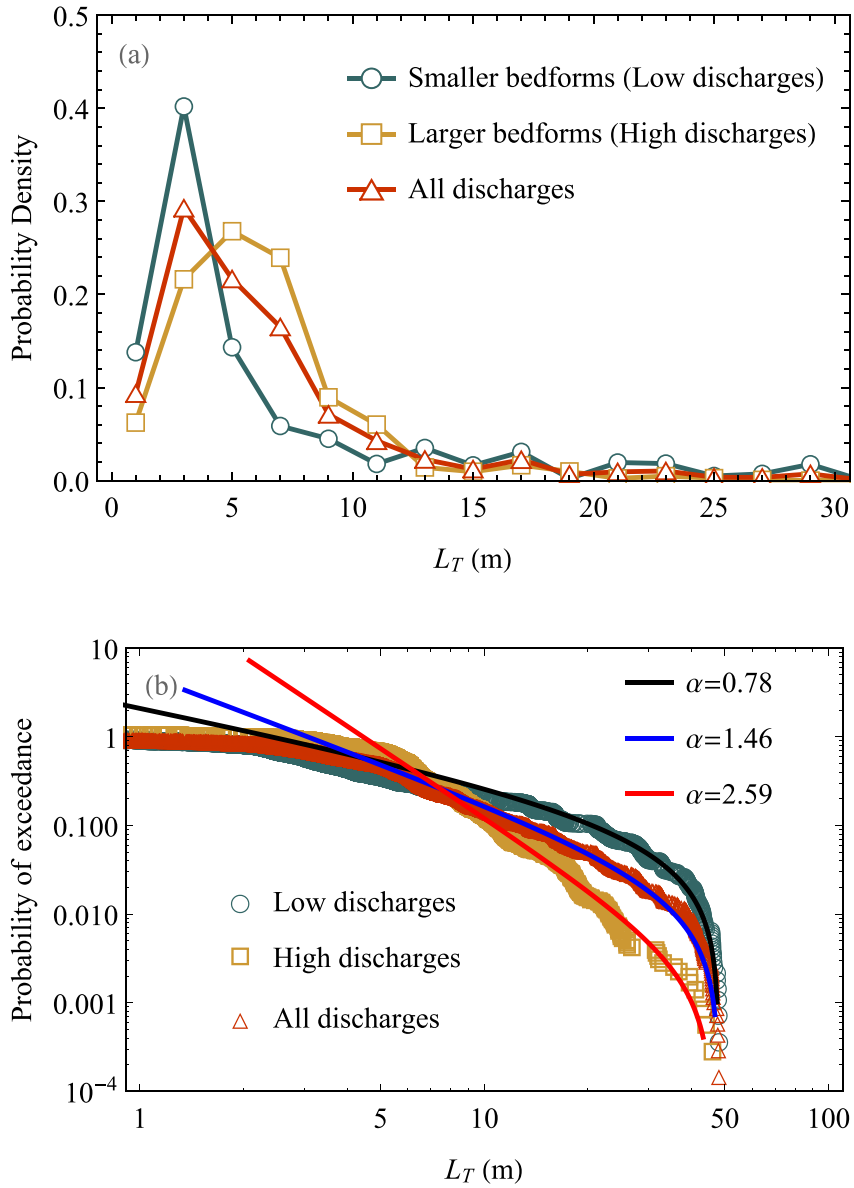

Figure 13. (a) Probability density functions, and (b) probability of exceedance of travel distances for the mixture of tracer particles for low discharges (open circles), high discharges (squares) and for all discharges (open triangles). The fitted truncated Pareto distributions are shown in solid lines in panel (b) and their parameters in Table 3.

The PDFs and probability of exceedances of the grouped travel distances for lower flows, higher flows, and all flows are shown in Figures 13a and 13b. From Figure 13b, we can see that the tail of the PDF is heavier for lower flows (circles) than for higher flows (squares). Notice the truncation at the streamwise location of ~50 m in Figure 13b, where all results drop sharply to zero representing the effect of limited length of the experimental flume. In addition, since more tracers (especially the larger grains) can move throughout the flume at the lower discharges (e.g., 600 and 800 L/s) compared with cases of higher discharges, which is straightforward as observed in Figures 8 and 12, the truncation effect is expected and seen to be more prominent for the results of green circles as shown in Figure 13b. Hence, the 50 m hard limit on travel distance makes a difference for the lower flows and not that much for the higher flows. Thus, "tail" in this case means the part of the curve approaching this length limit, but not affected by the truncation. In order to formally quantify the observed distribution, as well as separate and describe the tail characteristics, we adopted the truncated Pareto distribution, in which the physical constraint of the system can be revealed by the truncation parameter.

Table 3
Fitted Parameters of the Truncated Pareto Distribution

Q	α	Lower bound (γ) (m)	Upper bound (ν) (m)
Low discharge	0.78	6.82	48.1
High discharge	2.59	2.94	46.1
All discharges	1.46	6.46	48.1

The density of the truncated Pareto can be expressed as

$$f(x) = \frac{\alpha \gamma^{\alpha} x^{-\alpha-1}}{1-(\gamma/\nu)^{\alpha}}, \tag{7}$$

and its probability of exceedance is given by:

$$P(X > x) = \frac{\gamma^{\alpha}(x^{-\alpha} - \nu^{-\alpha})}{1-(\gamma/\nu)^{\alpha}} \tag{8}$$

where ν is the truncation parameter also called upper bound on the random variable X, α is the tail index and γ is the lower bound on the random variable X. More details about the truncated Pareto distribution and its fitting parameters can be found in Aban et al. (2006), Ganti et al. (2011), and Singh, Foufoula-Georgiou et al. (2012).

From the fitted truncated Pareto distributions (solid lines) to the low (circles) and the high flows (squares), it can be seen that the fitted parameter α is lower for the low flows (~0.8) whereas for the high flows it is ~2.5 (Table 3). The larger exponent α suggests a thinner tail such as an exponential or Gaussian type of decay in the case of high flows. The parameter ν (truncation parameter) suggests the finite length of the channel which is ~50 m, whereas the lower bound parameter γ suggests the average lengths of the bedforms, which are ~6 and ~3 m for low and high flows as discussed (Figure 2), respectively. Figure 13b (triangles) shows the exceedance probability of all the travel distances for all the discharges, approximating a real river system subjected to multiple flow regimes. The fitted parameter α (=1.46) suggests that the tail of the distribution in the case of a mixture of travel distances at all discharges and all size particles is heavier than that of the exponential or Gaussian distributions, thinner than that for plane beds, and heavier than that for beds with bedforms. Note the presence of a transition in the scaling regime (power-law regime of the PDF shape) at the bedform scale of ~6 m for the high flows.

A tail index of $\alpha = 0.78$ for the low discharge case (small bedforms) as shown in Figure 13b, suggests a heavy-tailed distribution, although we note that the characteristics of the "true tail" (the very end part of the distribution) remain unknown since the results are subjected to the effect of limited flume length, which truncates the possible heavy-tailed distribution and alters the tail behavior. That is, if the flume were much longer, the "true tail" may not keep decreasing in the manner of a power-law distribution with an index of $\alpha = 0.78$ and may eventually transition into a thin-tailed distribution (e.g., a so-called tempered power law distribution, Ganti et al. (2011); Meerschaert et al. (2008)). Recent studies for bedload transport (uniform particle size) with plane bed conditions also suggest similar results in that the step length distribution is most likely thin-tailed (Ancey & Heyman, 2014; Lajeunesse et al., 2010; Wu et al., 2020), arising from the physical constraints of limited flow strengths or velocities (Ancey & Heyman, 2014). On the other hand, our experiments suggest that the tradeoff between the effects of increasing discharge on increasing travel distances via stronger flow and decreasing travel distance via increased trapping in fact results in the thin-tailed distribution of travel distances, which is surprisingly much thinner than that for the condition of lower discharges. This result supports field observations of thin-tailed travel distances (Hassan et al., 2013).

5. Summary and Conclusions

This paper investigates the behavior of tracer particle movement in the presence of gravel bedforms in a large-scale experiment in a laboratory channel under different flow conditions. The data collected were high resolution measurements of spatial bed elevations and sediment transport rates along with travel distances of tracers of different grain size.

The main results of this study can be stated as follows:

1. The bedform geometry, extracted from the spatial bed elevation measurements, directly depends on discharge with increasing height, decreasing length, and decreasing variability in bedform aspect ratio as the discharge increases. A transition of bedforms from bedload sheets at lower discharge to low-amplitude dunes as the discharge increased was observed.
2. Measurements of tracer travel distances at multiple discharges show that tracer travel distances are primarily controlled by bedform structures. Trapping of tracer grains depends on the ratio of bedform height to tracer grain size (H_{bf}/D_t). Grains close to the median size of the bed may be trapped on the lee side of bedforms or in sheltered spots on the bed, whereas larger grains can roll further under the same flow conditions. With larger bedforms, all tracer grains tend to be trapped in the lee of bedforms, although some smaller grains may

preferentially overpass the bedforms at sufficiently high flow. These small grains may skip over a bedform wake via saltation and may have relatively large lateral motion following the near-bed current over lower elevations on the bedform crest.

3. To quantitatively characterize the ability of bedforms in trapping the particles, we calculated bedform trap efficiency based on 6,041 tracer-bedform encounters determined from mapping tracer trajectories and recording bedform passing and trapping. We find that the trap efficiency increases linearly with H_{bf}/D_t with 50% trap efficiency at $H_{bf}/D_t \sim 2$ and 90% trap efficiency for $H_{bf}/D_t \sim 4$. This pattern is consistent with an intuitive understanding that taller and steeper bedforms more readily trap grains.
4. As discharge increases, shear stress increases, producing longer travel distances, and bedform height increases, producing increased trapping potential. We observe that bedform trapping wins this competition, such that H_{bf}/D_t dominates the frequency and location of tracer deposition.
5. We adopted a tracer transport model based on the extended active layer formulation to test it against the observed travel distances. Our analysis shows that the analytical solution for travel distances can largely capture the distribution of tracer travel distance over all observed tracer sizes and discharges. This result can be seen as experimental evidence for the normal diffusion of bedload transport at small timescales as suggested by Wu, Singh, et al. (2019). Discrepancies between predicted and observed travel distances indicate enhanced tracer trap efficiency, such that the tracer transport model provides a reference against which bedform effects may be evaluated. "Preferential trapping" introduces a more deterministic element in the stochastic transport, which gives additional information regarding the spatial distributions of bedforms.
6. This work is the first experimental documentation of tracer travel distance for mixed grain size particles traversing a range of bedforms over multiple discharges, approximating conditions of natural rivers characterized by a wide range of grain size distributions and extreme flood events. The travel distance distribution of mixed particles under plane bed or small bedforms conditions shows heavy-tail characteristics to the extent allowed by the observational length of the flume. Increased bedform height and trapping efficiency acts to thin the tail of the travel distance distribution.
7. We show that migrating bedforms with height exceeding about three to four times the median size of the bed material have a substantial influence on tracer travel distance. This suggests that a predictive model of sediment transport should include a submodel for the occurrence, size, and migration rate of bedforms. Our results provide a starting point regarding the trapping efficiency of bedforms based on bedform height relative to grain size.

Data Availability Statement

The data used in the paper can be downloaded from https://doi.org/10.5281/zenodo.6703451.

Acknowledgments
This research was supported by the National Center for Earth-surface Dynamics (NCED), a Science and Technology Center funded by NSF under agreement EAR-0120914. A.S. acknowledges partial support from NSF EAR-1854452, Z.W. from National Natural Science Foundation of China (U2243222 and 52179067) and EFG from NSF EAR-1811909 and ECCS-1839441. We thank Tomas Georgiou, Nate Machtemes, Melissa Biegenwald, Craig Hill, Kristin Sweeney, Jim Mullin and Chris Ellis for helping with experimental design and data collection. We also thank the editor, associate editor and three anonymous reviewers whose suggestions and comments substantially improved our presentation and refined our interpretations.

References

Aban, I. B., Meerschaert, M. M., & Panorska, A. K. (2006). Parameter estimation for the truncated Pareto distribution. *Journal of the American Statistical Association*, *101*(473), 270–277. https://doi.org/10.1198/016214505000000411

Aberle, J., & Nikora, V. (2006). Statistical properties of armored gravel bed surfaces. *Water Resources Research*, *42*(11), W11414. https://doi.org/10.1029/2005wr004674

Ancey, C. (2010). Stochastic modeling in sediment dynamics: Exner equation for planar bed incipient bed load transport conditions. *Journal of Geophysical Research*, *115*(F2), F00A11. https://doi.org/10.1029/2009jf001260

Ancey, C., Davison, A., Böhm, T., Jodeau, M., & Frey, P. (2008). Entrainment and motion of coarse particles in a shallow water stream down a steep slope. *Journal of Fluid Mechanics*, *595*, 83–114. https://doi.org/10.1017/s0022112007008774

Ancey, C., & Heyman, J. (2014). A microstructural approach to bed load transport: Mean behaviour and fluctuations of particle transport rates. *Journal of Fluid Mechanics*, *744*, 129–168. https://doi.org/10.1017/jfm.2014.74

Bradley, D. N. (2017). Direct observation of heavy-tailed storage times of bed load tracer particles causing anomalous superdiffusion. *Geophysical Research Letters*, *44*(24), 227–235. https://doi.org/10.1002/2017gl075045

Chacho, E., Burrows, R., & Emmett, W. (1989). Detection of coarse sediment movement using radio transmitters. In *Paper presented at international association for hydraulic research XXIII congress*.

Church, M., & Hassan, M. A. (1992). Size and distance of travel of unconstrained clasts on a streambed. *Water Resources Research*, *28*(1), 299–303. https://doi.org/10.1029/91wr02523

Dinehart, R. L. (1992). Evolution of coarse gravel bed forms: Field measurements at flood stage. *Water Resources Research*, *28*(10), 2667–2689. https://doi.org/10.1029/92WR01357

Einstein, H. (1937). *Bedload transport as a probability problem. Sedimentation* (pp. 105–108). Water Resources Publications. (reprinted in 1972).

Einstein, H. A. (1950). *The bed-load function for sediment transportation in open channel flows*. US Department of Agriculture.

Ergenzinger, P., Schmidt, K. H., & Busskamp, R. (1989). The pebble transmitter system (PETS): First results of a technique for studying coarse material erosion, transport and deposition. *Zeitschrift für Geomorphologie*, *33*(4), 503–508. https://doi.org/10.1127/zfg/33/1989/503

Foley, M. G. (1977). Gravel-lens formation in antidune-regime flow; a quantitative hydrodynamic indicator. *Journal of Sedimentary Research*, *47*(2), 738–746.
Furbish, D. J., Haff, P. K., Roseberry, J. C., & Schmeeckle, M. W. (2012). A probabilistic description of the bed load sediment flux: 1. Theory. *Journal of Geophysical Research*, *117*(F3), F03031. https://doi.org/10.1029/2012jf002352
Ganti, V., Meerschaert, M. M., Foufoula-Georgiou, E., Viparelli, E., & Parker, G. (2010). Normal and anomalous diffusion of gravel tracer particles in rivers. *Journal of Geophysical Research*, *115*(F2), F00A12. https://doi.org/10.1029/2008jf001222
Ganti, V., Singh, A., Passalacqua, P., & Foufoula-Georgiou, E. (2009). Subordinated Brownian motion model for sediment transport. *Physical Review E*, *80*(1), 011111. https://doi.org/10.1103/physreve.80.011111
Ganti, V., Straub, K. M., Foufoula-Georgiou, E., & Paola, C. (2011). Space-time dynamics of depositional systems: Experimental evidence and theoretical modeling of heavy-tailed statistics. *Journal of Geophysical Research*, *116*(F2), F02011. https://doi.org/10.1029/2010jf001893
Gomez, B., Naff, R. L., & Hubbell, D. W. (1989). Temporal variations in bedload transport rates associated with the migration of bedforms. *Earth Surface Processes and Landforms*, *14*(2), 135–156. https://doi.org/10.1002/esp.3290140205
Habersack, H. M. (2001). Radio-tracking gravel particles in a large braided river in New Zealand: A field test of the stochastic theory of bed load transport proposed by Einstein. *Hydrological Processes*, *15*(3), 377–391. https://doi.org/10.1002/hyp.147
Hassan, M. A. (1990). Scour, fill, and burial depth of coarse material in gravel bed streams. *Earth Surface Processes and Landforms*, *15*(4), 341–356. https://doi.org/10.1002/esp.3290150405
Hassan, M. A., & Bradley, D. N. (2017). Geomorphic controls on tracer particle dispersion in gravel-bed rivers. In D. Tsutsumi & J. B. Laronne (Eds.), *Gravel-bed rivers*. https://doi.org/10.1002/9781118971437.ch6
Hassan, M. A., Church, M., & Schick, A. P. (1991). Distance of movement of coarse particles in gravel bed streams. *Water Resources Research*, *27*(4), 503–511. https://doi.org/10.1029/90wr02762
Hassan, M. A., Voepel, H., Schumer, R., Parker, G., & Fraccarollo, L. (2013). Displacement characteristics of coarse fluvial bed sediment. *Journal of Geophysical Research: Earth Surface*, *118*(1), 155–165. https://doi.org/10.1029/2012jf002374
Hill, K. M., DellAngelo, L., & Meerschaert, M. M. (2010). Heavy-tailed travel distance in gravel bed transport: An exploratory enquiry. *Journal of Geophysical Research*, *115*(F2), F00A14. https://doi.org/10.1029/2009jf001276
Hubbell, D., & Sayre, W. W. (1964). Sand transport studies with radioactive tracers. *Journal of the Hydraulics Division*, *90*(3), 39–68. https://doi.org/10.1061/jyceaj.0001057
Keylock, C. J., Singh, A., & Foufoula-Georgiou, E. (2014). The complexity of gravel bed river topography examined with gradual wavelet reconstruction. *Journal of Geophysical Research: Earth Surface*, *119*(3), 682–700. https://doi.org/10.1002/2013jf002999
Kleinhans, M. G., & Rijn, L. C. V. (2002). Stochastic prediction of sediment transport in sand-gravel bed rivers. *Journal of Hydraulic Engineering*, *128*(4), 412–425. https://doi.org/10.1061/(asce)0733-9429(2002)128:4(412)
Lajeunesse, E., Malverti, L., & Charru, F. (2010). Bed load transport in turbulent flow at the grain scale: Experiments and modeling. *Journal of Geophysical Research*, *115*(F4), F04001. https://doi.org/10.1029/2009jf001628
Li, G., Gong, Z., Jiang, W., Zhan, J., Wang, B., Fu, X., et al. (2023). Environmental transport of gyrotactic microorganisms in an open-channel flow. *Water Resources Research*, *59*(4), e2022WR033229. https://doi.org/10.1029/2022WR033229
Lisle, I. G., Rose, C. W., Hogarth, W. L., Hairsine, P. B., Sander, G. C., & Parlange, J. Y. (1998). Stochastic sediment transport in soil erosion. *Journal of Hydrology*, *204*(1), 217–230. https://doi.org/10.1016/s0022-1694(97)00123-6
Mao, L., Cooper, J. R., & Frostick, L. E. (2011). Grain size and topographical differences between static and mobile armour layers. *Earth Surface Processes and Landforms*, *36*(10), 1321–1334. https://doi.org/10.1002/esp.2156
Martin, R. L., Jerolmack, D. J., & Schumer, R. (2012). The physical basis for anomalous diffusion in bed load transport. *Journal of Geophysical Research*, *117*(F1), F01018. https://doi.org/10.1029/2011jf002075
McEwan, I., Sørensen, M., Heald, J., Tait, S., Cunningham, G., Goring, D., & Willetts, B. (2004). Probabilistic modeling of bed-load composition. *Journal of Hydraulic Engineering*, *130*(2), 129–139. https://doi.org/10.1061/(asce)0733-9429(2004)130:2(129)
Meerschaert, M. M., & Scheffler, H. P. (2001). *Limit distributions for sums of independent random vectors: Heavy tails in theory and practice*. John Wiley & Sons.
Meerschaert, M. M., Zhang, Y., & Baeumer, B. (2008). Tempered anomalous diffusion in heterogeneous systems. *Geophysical Research Letters*, *35*(17), L17403. https://doi.org/10.1029/2008gl034899
Nelson, P. A., Venditti, J. G., Dietrich, W. E., Kirchner, J. W., Ikeda, H., Iseya, F., & Sklar, L. S. (2009). Response of bed surface patchiness to reductions in sediment supply. *Journal of Geophysical Research*, *114*(F2), F02005. https://doi.org/10.1029/2008jf001144
Nikora, V., Habersack, H., Huber, T., & McEwan, I. (2002). On bed particle diffusion in gravel bed flows under weak bed load transport. *Water Resources Research*, *38*(6), 17-1–17-9. https://doi.org/10.1029/2001wr000513
Orr, C. H., Clark, J. J., Wilcock, P. R., Finlay, J. C., & Doyle, M. W. (2009). Comparison of morphological and biological control of exchange with transient storage zones in a field-scale flume. *Journal of Geophysical Research*, *114*(G2), G02019. https://doi.org/10.1029/2008jg000825
Paintal, A. (1971). A stochastic model of bed load transport. *Journal of Hydraulic Research*, *9*(4), 527–554. https://doi.org/10.1080/00221687109500371
Pelosi, A., Schumer, R., Parker, G., & Ferguson, R. (2016). The cause of advective slowdown of tracer pebbles in rivers: Implementation of exner based master equation for coevolving streamwise and vertical dispersion. *Journal of Geophysical Research: Earth Surface*, *121*(3), 623–637. https://doi.org/10.1002/2015jf003497
Phillips, C. B., Martin, R. L., & Jerolmack, D. J. (2013). Impulse framework for unsteady flows reveals superdiffusive bed load transport. *Geophysical Research Letters*, *40*(7), 1328–1333. https://doi.org/10.1002/grl.50323
Pierce, J. K., & Hassan, M. A. (2020a). Back to Einstein: Burial-induced three-range diffusion in fluvial sediment transport. *Geophysical Research Letters*, *47*(15), e2020GL087440. https://doi.org/10.1029/2020GL087440
Pierce, J. K., & Hassan, M. A. (2020b). Joint stochastic bedload transport and bed elevation model: Variance regulation and power law rests. *Journal of Geophysical Research: Earth Surface*, *125*(4), e2019JF005259. https://doi.org/10.1029/2019JF005259
Pretzlav, K. L. G., Johnson, J. P. L., & Bradley, D. N. (2021). Smartrock transport from seconds to seasons: Shear stress controls on gravel diffusion inferred from hop and rest scaling. *Geophysical Research Letters*, *48*(9), e2020GL091991. https://doi.org/10.1029/2020GL091991
Pyrce, R. S., & Ashmore, P. E. (2003). Particle path length distributions in meandering gravel-bed streams: Results from physical models. *Earth Surface Processes and Landforms*, *28*(9), 951–966. https://doi.org/10.1002/esp.498
Pyrce, R. S., & Ashmore, P. E. (2005). Bedload path length and point bar development in gravel-bed river models. *Sedimentology*, *52*(4), 839–857. https://doi.org/10.1111/j.1365-3091.2005.00714.x
Ranjbar, S., & Singh, A. (2020). Entropy and intermittency of river bed elevation fluctuations. *Journal of Geophysical Research: Earth Surface*, *125*(8), e2019JF005499. https://doi.org/10.1029/2019jf005499

Roseberry, J. C., Schmeeckle, M. W., & Furbish, D. J. (2012). A probabilistic description of the bed load sediment flux: 2. Particle activity and motions. *Journal of Geophysical Research*, *117*(F3), F03032. https://doi.org/10.1029/2012jf002353

Sayre, W. W., & Hubbell, D. W. (1965). *Transport and dispersion of labeled bed material*. US Government Printing Office.

Singh, A., Fienberg, K., Jerolmack, D. J., Marr, J., & Foufoula-Georgiou, E. (2009). Experimental evidence for statistical scaling and intermittency in sediment transport rates. *Journal of Geophysical Research*, *114*(F1), F01025. https://doi.org/10.1029/2007jf000963

Singh, A., Foufoula-Georgiou, E., Porté-Agel, F., & Wilcock, P. R. (2012). Coupled dynamics of the co-evolution of gravel bed topography, flow turbulence and sediment transport in an experimental channel. *Journal of Geophysical Research*, *117*(F4), F04016. https://doi.org/10.1029/2011jf002323

Singh, A., Guala, M., Lanzoni, S., & Foufoula-Georgiou, E. (2012). Bedform effect on the reorganization of surface and subsurface grain size distribution in gravel bedded channels. *Acta Geophysica*, *60*(6), 1607–1638. https://doi.org/10.2478/s11600-012-0075-z

Singh, A., Lanzoni, S., & Foufoula-Georgiou, E. (2009). Nonlinearity and complexity in gravel bed dynamics. *Stochastic Environmental Research and Risk Assessment*, *23*(7), 967–975. https://doi.org/10.1007/s00477-008-0269-8

Singh, A., Lanzoni, S., Wilcock, P. R., & Foufoula-Georgiou, E. (2011). Multiscale statistical characterization of migrating bed forms in gravel and sand Bed Rivers. *Water Resources Research*, *47*(12), W12526. https://doi.org/10.1029/2010wr010122

Singh, A., Porté-Agel, F., & Foufoula-Georgiou, E. (2010). On the influence of gravel bed dynamics on velocity power spectra. *Water Resources Research*, *46*(4), W04509. https://doi.org/10.1029/2009wr008190

Whiting, P. J., Dietrich, W. E., Leopold, L. B., Drake, T. G., & Shreve, R. L. (1988). Bedload sheets in heterogeneous sediment. *Geology*, *16*(2), 105–108. https://doi.org/10.1130/0091-7613(1988)016<0105:bsihs>2.3.co;2

Wilcock, P. R. (1997). Entrainment, displacement and transport of tracer gravels. *Earth Surface Processes and Landforms*, *22*(12), 1125–1138. https://doi.org/10.1002/(sici)1096-9837(199712)22:12<1125::aid-esp811>3.0.co;2-v

Wong, M., Parker, G., DeVries, P., Brown, T. M., & Burges, S. J. (2007). Experiments on dispersion of tracer stones under lower-regime plane-bed equilibrium bed load transport. *Water Resources Research*, *43*(3), W034403. https://doi.org/10.1029/2006wr005172

Wu, Z., Foufoula-Georgiou, E., Parker, G., Singh, A., Fu, X., & Wang, G. (2019). Analytical solution for anomalous diffusion of bedload tracers gradually undergoing burial. *Journal of Geophysical Research: Earth Surface*, *124*(1), 21–37. https://doi.org/10.1029/2018jf004654

Wu, Z., Furbish, D., & Foufoula-Georgiou, E. (2020). Generalization of hop distance-time scaling and particle velocity distributions via a two-regime formalism of bedload particle motions. *Water Resources Research*, *56*(1), e2019WR025116. https://doi.org/10.1029/2019wr025116

Wu, Z., Jiang, W., Zeng, L., & Fu, X. (2023). Theoretical analysis for bedload particle deposition and hop statistics. *Journal of Fluid Mechanics*, *954*, A11. https://doi.org/10.1017/jfm.2022.959

Wu, Z., Singh, A., Foufoula-Georgiou, E., Guala, M., Fu, X., & Wang, G. (2021). A velocity-variation-based formulation for bedload particle hops in rivers. *Journal of Fluid Mechanics*, *912*(A33), A33. https://doi.org/10.1017/jfm.2020.1126

Wu, Z., Singh, A., Fu, X., & Wang, G. (2019). Transient anomalous diffusion and advective slowdown of bedload tracers by particle burial and exhumation. *Water Resources Research*, *55*(10), 7964–7982. https://doi.org/10.1029/2019wr025527

Yarnell, S. M., Mount, J. F., & Larsen, E. W. (2006). The influence of relative sediment supply on riverine habitat heterogeneity. *Geomorphology*, *80*(3–4), 310–324. https://doi.org/10.1016/j.geomorph.2006.03.005